Femtosecond laser micro-patterning of optical properties and functionalities in novel photosensitive silver-containing fluorophosphate glasses

Tarcio de Castro, Hssen Fares, Alain Abou Khalil, Romain Laberdesque, Yannick Petit, Clément Strutinski, Sylvain Danto, Veronique Jubera, Sidney J. L. Ribeiro, Marcelo Nalin, et al.

Femtosecond laser micro-patterning of optical properties and functionalities in novel photosensitive silver-containing fluorophosphate glasses

Tarcio de Castro,[1,2] Hssen Fares,[1,2] Alain Abou Khalil,[3] Romain Laberdesque,[3] Yannick Petit,[2,3,*] Clément Strutinski,[2] Sylvain Danto,[2] Véronique Jubera,[2] Sidney J. L. Ribeiro,[1] Marcelo Nalin,[1] Thierry Cardinal[3], and Lionel Canioni[3].

[1] Institute of Chemistry, São Paulo State University, UNESP, Araraquara-SP, Brazil.

[2] University of Bordeaux, CNRS, ICMCB, UPR 9048, 87 avenue du Dr. A. Schweitzer, 33608 Pessac cedex, France.

[3] University of Bordeaux, CNRS, CEA, CELIA, UMR 5107, 351 Cours de la Libération, 33405 Talence Cedex, France.

Corresponding author: yannick.petit@u-bordeaux.fr

Abstract Silver-containing glasses are promising candidates for photonic applications, due to the potentiality of spectroscopic properties of silver nanoclusters (NC's) and/or silver metallic nanoparticles. In this framework, silver-containing fluorophosphate glasses are candidates with a strong potential. Indeed, combined with femtosecond laser irradiation, silver NC's may be tailored in three-dimensional fluorescent micro-structures, whose spectroscopic properties have been investigated, revealing the creation of silver NC's but also of NP's during laser irradiation in the studied fluorophosphate glass. Additionally, the photo-inscription of silver NC's is correlatively accompanied by a positive index change, which has led to the demonstration of optical waveguiding behavior. Finally, the management of the reservoir of available silvers for laser inscription is investigated. Unlike previous observations made in standard oxide phosphate glasses, the considered silver-containing fluorophosphate glass exhibes an intriguing ability to be re-written when subjected to successive overlapping laser irradiations. Upon the optimization of compositions with tailored photo-sensitivity, the re-writable ability of fluorophosphate glasses paves the way to the design of advanced photonic devices such as photonic optical circuits, evanescent sensors or 3D high-density optical data storage.

1. Introduction

Direct laser writing (DLW) has become for the two last decades a suitable technique for three-dimensional (3D) micro- and even nano-structuring of physico-chemical and optical properties, which is at the root of remarkable photonic functionalities [1-3]. Although standard materials allow for remarkable laser-induced behaviors, prepared materials with compositions specifically designed for femtosencond (fs) laser interaction appear as a promising alternative [4-6]. These materials, among which prepared glasses with rare earth ions or noble metal ions, can provide an enhanced sensitivity [7], requiring thus a lower amount of deposited dose (lower laser irradiance or lower number of pulses) [8]. Beyond, prepared glasses such as silver-containing glasses can also give access to a large panel of laser-induced optical responses at different scales, spanning from the sub-micron to the macroscopic scale [8,9]. Silver-containing glasses, with silver species such as metal ions Ag^+, nanoclusters (Ag NC's) and/or nanoparticles (Ag NP's), become candidates for photonic applications in light sources [10], second-harmonic generation [11-13], laser illumination [14], white light generation [15] or photonic integrated circuits based on waveguides [16,17]. Such potentiality of Ag NC's and NP's is partially due to their tunable spectral properties that strongly depend on their size, geometries and spatial distributions [18]. This is commonly controlled either by the concentration, melting temperature and thermal treatment in the case of statistically-homogeneous pristine materials [19], or by the appropriate femtosecond laser irradiation which leads to 3D multiscale photonic architectures, as observed in a large panel of glasses [5,8,20-23].

To date, most of femtosecond laser structuring progresses have been performed in oxide silver-containing glasses, including sodocalcite or borosilicate glasses [23] and mostly phosphate glasses [5,8,12,13,17,22-23]. In the meantime, silver-containing fluorophosphate glasses have gained very limited attention with respect to DLW. Recently, Fares *et al.* have demonstrated the feasibility of Ag NC's doped fluorophosphate glasses for waveguide inscription, operating a Ti:Saphire laser at 800 nm [26]. Besides, thanks to the low viscosity allowed by the phosphate groups, these vitreous systems own a large metal solubility. Additionally, fluorophosphate glasses present significant chemical

durability due to insoluble fluorides. They exhibit also low melting point temperature, stability against devitrification and low glass transition [27,28]. As compared to silver-containing phosphate glasses, silver-containing fluoro phosphate systems represent an interesting new field of investigation for femtosecond laser irradiation and activation of silver photochemistry, to potentially access enhanced photosensitivity and/or new optical properties.

In this article, we present the synthesis of a considered silver-containing fluorophosphate glass and the characterization of its pristine fluorescence spectroscopic properties linked to silver species. Then, we demonstrated for the first time that the interaction of a near-IR fs pulsed laser with this material leads to 3D micron-scale patterned structures with a strong fluorescent contrast. The Ag NC's created by DLW are shown to be well-organized along a double-track fluorescent structure that locally exhibits a positive index change, which sustains a waveguiding behavior. Finally, the management of silver reservoir is addressed by performing successive laser irradiations with increasing overlapping, emphasizing an original and intriguing re-writable behavior compared to standard phosphate glasses.

2. Experimental Procedure

2.1 Glass synthesis and characterization

The glass sample with molar composition $46.2NaPO_3$-$25.6MgF_2$-$15.4CdF_2$-$10.2YF_3$-$2.6Ag_2O$ (mol%) was prepared by the melt-quenching method using high purity raw materials. A series of mixed batches (8 grams each) was melted in an alumina crucible at 900 °C for 45 min under air atmosphere, and then pourred out and annealed for 2 hours in a stainless steel mold preheated at 40 °C below the glass transition (T_g ~ 363 °C).

Thermal analysis was performed by differential thermal analysis (DSC 2920 TA Instruments) with 30 mg samples. The measurements were performed at temperatures ranging from 200 to 700 °C with a heating rate of 10 °C/min. X-ray diffraction (XRD) was performed with the Cu-K_α radiation (λ = 0.15418 nm) and the associated pattern was collected on a PANalitycal X'pert

MPD-PRO Bragg-Brentano θ-θ geometry equipped with a secondary monochromator and X'Celerator multi-strip detector over an angular range of 2θ = 8–80 °. The density ρ was determined by the Archimedes method using distilled water as immersion liquid with an error of 0.0001 g/cm^3.

The refractive index *n* was measured using M-line prism coupling technique at 633 nm. The UV-Vis transmission spectrum was recorded using a Cary 5000 (Varian) spectrometer with a polished sample of 500 µm thickness, from 200 nm to 800 nm with a step of 1 nm. Excitation and emission spectra were collected with a fluorimeter (Fluorolog Horiba Jobin Yvon) equipped with a Xenon lamp (450W) and a photomultiplier tube (Ramamatsu R298) at room temperature on glass powder.

2.2 Femtosecond laser inscription procedure and laser-induced structures

For DLW inscription, the sample was cut as a parallelepiped-shaped piece with dimensions of 7×4×2 mm^3, and then polished to optical quality. The experimental setup for DLW was composed by a home-made nonlinear microscope combined with a KGW:Yb fs oscillator (Amplitude System, up to 2.6 W average power, 9.8 MHz repetition rate, 390 fs pulse duration (FWHM), and operating at 1030 nm). The laser irradiance was controlled with an acousto-optics modulator enabling the controled accumulation up to N = 10^6 pulses, and energy pulses spanning from 20 nJ to 150 nJ at the laser beam voxel in the glass. The laser beam was focused perpendicularly to the surface of the sample using a microscope objective (Carl Zeiss, 20× – 0.75 NA), at the typical depth of 160 µm below the glass surface. The displacements along the *xyz* axes were carried out with a high precision 3D translation stage (XMS-50 stages, Micro Controler).

By using back-and-forth displacements, 12 patterned structures were inscribed with different laser parameters. Three writing speeds were applied: 10, 50 and 100 µm/s, respectively corresponding to 1.7×10^6, 3.3×10^5 and 1.7×10^5 deposited pulses, while the irradiance varied from 9 to 13.5 TW/cm^2 at the beam focus in the sample. For the waveguide inscription, a longitudinal line was drawn with speed of 300 µm/s. The mode profile of the WG was carried out using a red laser diode emitting at 630 nm. The signal of the guided light was collected by an

objective (100× – 0.55NA Mitutoyo) accopled on a CCD camera. The refractive index change of the written waveguide was measured using a commercially available wave-front sensor SID4Bio by Phasics Inc. The wave-front sensor is placed in a microscope operating in transmission mode under white light illumination. A 100x-1.3NA oil objective is used to visualize and acquire the phase image of the waveguide. The refractive index change could be then retrieved from the phase image by dividing the optical path difference (measured by the SID4Bio) by the thickness of the waveguide (typically, 6 µm thick).

Additional DLW was performed by back-and-forth displacements, with three distinct interdistances between each pass, namely 5 µm, 1 µm and 0.5 µm, with sample velocity of 100 µm/s and typically 10 TW/cm^2 peak irradiance. The interdistances of 1 µm and 0.5 µm were clearly smaller than the typical Gaussian beam diameter of 1.6 µm (full width at e^{-2} = 13.6%). These structures were then imaged with a Leica fluorescence microscope in wide field mode (excitation at 375 nm and collection with an Olympus objective: 20× – 0.75 NA). DLW and fluorescence imaging of a standard silver-containing oxide phosphate glass are included for comparing the silver reservoir management during overlapping DLW and to discuss the similarities and differences in the re-writing behavior of these two glasses.

3. Results and discussion

3.1 Glass properties

The DSC analysis is displayed in Fig.1(a). A typical glass transition T_g = 363 ± 2°C is followed by an exothermic peak centered at 545 ± 2°C. The onset of crystallization temperature is estimated at T_x = 520 ± 2°C, which attests a high thermal stability against devitrification ($\Delta T = T_x - T_g$ = 157 °C) and thus makes this composition a potential candidate for fiber drawing. The absorption spectrum of the glass along with the micrograph of a sample is depicted in Fig.1 (b).

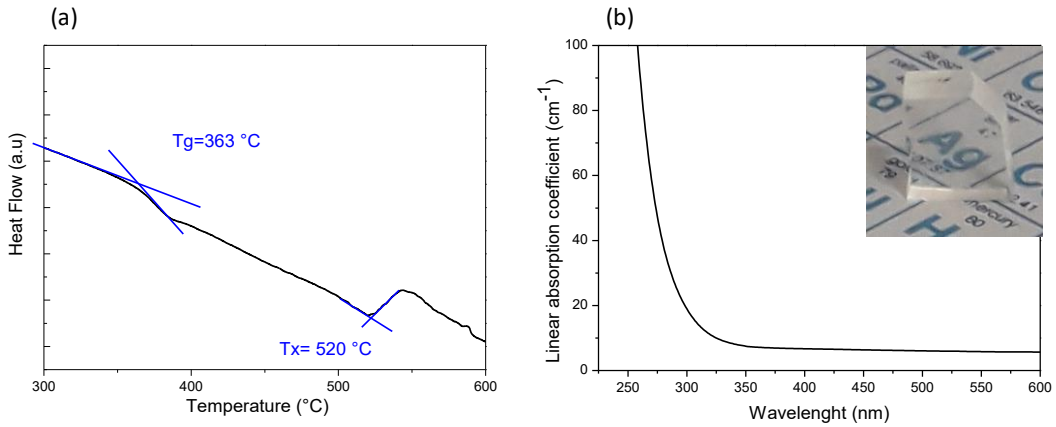

Figure 1. (a) DSC scan of the silver-containing fluorophosphate glass showing the glass transition and crystallization temperatures; (b) associated absorption spectrum.

The physicochemical properties of the considered fluorophosphate glass and of a standard silver-containing oxide phosphate glass, including their compositions, glass transition and crystallization temperature, density, refractive index and cut-off wavelengths, are reported in Table 1.

Table 1. Investigated glasses and related properties

Samples	Composition (mol%)	T_g (°C) [± 2 °C]	T_x (°C) [± 2 °C]	ρ ($g.cm^{-3}$)	n [± 0.001]	$\lambda_{Cut\text{-}off}$ (nm)
Oxi-fluoride phosphate	$46.2NaPO_3$-$25.6MgF_2$-$15.4CdF_2$-$10.2YF_3$-$2.6Ag_2O$	363	520	2.904	1.58 (at 632 nm)	280
Phosphate	$40P_2O_5$-55ZnO-$1Ga_2O_3$-$4Ag_2O$	396	-	3.533	1.59 (at 656 nm)	270

The photoluminescence excitation and emission properties of the silver-containing fluorophosphate glass sample are shown in Figs. 2(a) and 2(b), respectively. Excitation spectra shows two broad excitation bands (typically positioned at 270 and 350 nm), that undergo a red-shift from UV towards the visible range for emissions being collected at 400 nm, 450 nm and 500 nm (Fig. 2(a)). Excitation spectra shifts to longer wavelength for emission collection at longer wavelengths. Correlatively, excitations at longer wavelengths, at respectively 260 nm, 300 nm and 350 nm, lead to red-shifted emission spectra, as shown in Fig. 2(b). This dependence of the Ag NC's fluorescence properties

match well the behavior reported in other host fluorophosphate glass matrices, in which a strong relationship between the excitation wavelengths and the size of Ag NC's is highlighted [29-31]. In this sense, the observed fluorescence profiles in Fig. 2 suggests a distribution of distinct Ag NC's with different sizes and/or geometries in accordance with previous study on fluorophosphate glass [32] . It is worth mentioning that, as reported by Tikhomirov *et al.* [32], the F^- vacancies located in the amorphous matrix could act as nucleation centers by attracting Ag^+ ions, resulting in the formation of distinct Ag NC's.

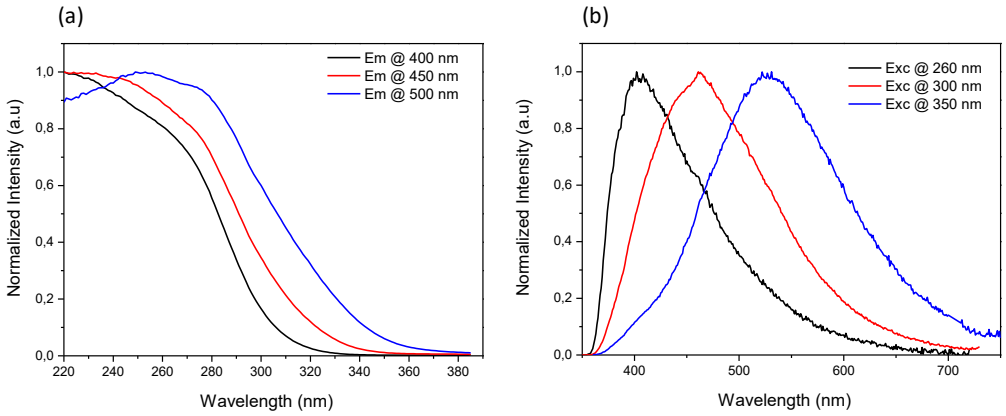

Figure 2. (a) Photoluminescence excitation spectra of silver-containing fluorophosphate glass collected at different fluorescence emissions; (b) Photoluminescence emission spectra for different excitation wavelengths.

3.2 Micro-patterning of Ag NC's

The principle of DLW interaction is depicted in Fig. 3(a). The custom-built laser inscription setup performs back-and-forth motions that produces patterns with dimensions of 100×100 μm^2 for different irradiances and pulses number accumulation. Highly-fluorescent structures can be seen by naked eyes while excited under UV radiation (at 355 nm in this case), as shown by the digital micrograph in Fig. 3(b). Interestingly, during the DLW process, a fraction of the Ag^+ ions can be reduced by the photo-induced ejected free electrons produced by multi-photon absorption mostly in the central part of the beam. Then, the photo-induced pulse-to-pulse cumulative energy deposition is accompanied by a cationic diffusion with the radial drift of silver ions Ag^+ and neutral silver elements

Ag^0, which leads to the formation of highly fluorescent Ag_m^{x+} species, as shown in Fig. 3(c). Such Ag_m^{x+} species are formed around the interaction voxel [4,5,23]. The overall produced silver clusters and associated size distribution depends both on the amount of deposited energy at the laser voxel, on the efficiency of the photoactivated migration of silver species and on the resulting photochemistry to grow silver clusters, but also on the pre-existing silver clusters in the pristine glass that can be further grown by the fs laser irradiation. Fig. 3(c) shows a wide-field fluorescence image (excitation at 405 nm) of various laser-created bright fluorescent structures for different writing parameters. The laser irradiation condition with the larger amount of cumulated pulses (speed of 10 µm/s) leads to micro-patterned Ag NC's that show the brightest fluorescence, compared to structures produced at lower velocities. As observed in phosphate glasses [22,24], deposited doses with increasing irradiances typically lead to more intense fluorescence emissions. The geometry of silver cluster distribution, not resolved in Fig. 3(c), is further detailed in Fig. 4.

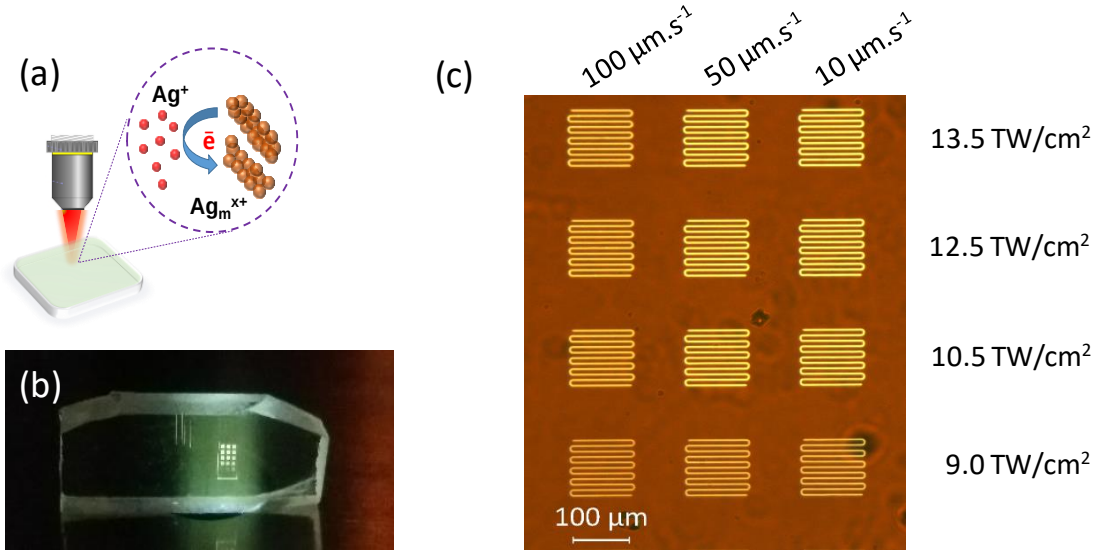

Figure 3. (a) Scheme of the silver cluster creation and growth around the fs laser beam voxel; (b) micrograph of the silver-containing fluorophosphate glass under UV light exposure (excitation at 355 nm); (c) fluorescence microscope image with wide-field illumination with UV light (excitation at 405 nm) of all the 3D-localized produced patterns showing 100×100 µm^2 lateral dimensions with 10 µm interline separation.

Differential micro-transmission spectroscopy of the laser-induced patterns of Fig. 3(c) was recorded with respect to the pristine glass. Measurements were obtained by a spatial integration over a 50×50 μm^2 square, so that the provided spectra are spatially averaged. Such spectra were converted into differential micro-extinction spectra, revealing that the photoinduced Ag NC's show a broad absorption bands (as seen in Fig. 4(a)) and a remarkably broadband emission over the visible range (not shown here). In such representation, a pristine glass area shows a null differential micro-extinction behavior. The extinction becomes more intense while reducing velocities from 100 µm/s to 50 µm/s, and much more intense and broader at 10 µm/s, which indicates that laser-induced silver NC's evolve both in concentration and size with the irradiation parameters. Indeed, the pattern corresponding to laser irradiation parameters of 10 µm/s and 13.5 TW/cm^2 shows a micro-extinction with a maximum at 370 nm and a long extension up to 650 nm. However, the extinction spectra (Fig. 4) differs from the excitation spectra (Fig. 2(a)), showing a wider response in the visible region. This extension results in two aspects: (i) the laser-induced creation of larger Ag NC's than those contained in the pristine glass, and (ii) the production of absorbing but non-emitting metallic Ag NP's with surface plasmonic resonance. Differential micro-extinction has been analyzed for the laser irradiation parameters of 10 µm/s and 13.5 TW/cm^2, with a proper fit in the 300 nm – 650 nm range with a three-Gaussian model (Fig. 4(b)). Spectra below 300 nm could not be recorded, even though such UV range surely contains laser-induced absorption and thus excitation bands, similarly to the ones discussed in detail by Marquestaut *et al.* in the case of a silver-containing phosphate glass [**33**]. The present modeling for the considered silver-containing fluorophosphate glass shows first a band centered at 340 nm attributed to laser-induced clusters, labeled here Ag_α, to specify that such silver NC's are not identified in detail except that they were not present in the pristine glass. Second, the model shows a band centered at about 387 nm attributed to neutral silver atoms Ag^0, similarly to [**33**]. Finally, the third band is attributed to the surface plasmonic resonance band, centered at 450 nm. The latter band grows remarkably while reducing the sample velocity, allowing stronger thermal cumulative and growth of silver species from NC's to NP's. The spectral parameters of the modeling are gathered in Table 2. It is worth noting that the extinction spectra correspond to very high linear absorption coefficients.

Indeed, with the considered irradiation conditions, the thickness of the laser-induced structures typically corresponds to 6 µm. The spatially-averaged laser-induced differential linear absorption coefficient typically equals 0.3/6 ~0.05 μm^{-1} ~ 500 cm^{-1}. Moreover, each laser pass generates two fluorescent walls made of silver NC's, typically separated of 1.8 µm and with an hypothetical individual thickness of e = 200 nm (not resolved in Fig. 3(c) but better resolved in Fig. 5, similarly to [**34**]). Considering that laser passes were distant of d = 10 µm, the local differential linear absorption coefficient equals $500/(2e/d) \sim 12500\ cm^{-1}$, demonstrating very intense absorption properties of the laser-induced NC's and/or NP's. The local concentration of silver species being extremely difficult to determine, the individual absorption cross-section is not reachable at the stage.

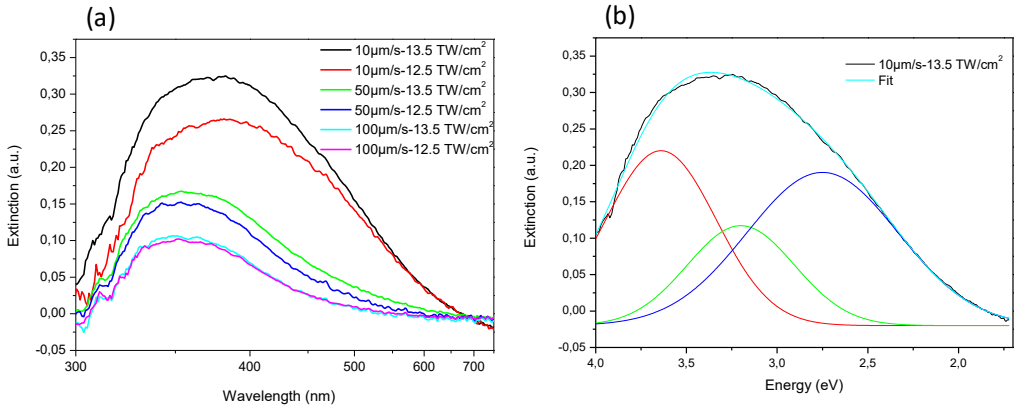

Figure 4. (a) Differential micro-extinction spectra showing spatially-averaged behavior of several patterns among those from Fig. 3(c), created with distinct laser irradiation conditions; (b) Appropriate modeling of the most intense extinction spectrum (laser irradiation condition at 10 µm/s, 13.5 TW/cm^2), with a three-Gaussian band model showing the laser-induced metallic silver NP's surface plasmonic resonance band at 2.75 eV (450 nm).

Table 2. Identification and labeling of laser-induced silver species and associated absorption bands

Ag Species	Position [ev]	Position [nm]	FWHM [ev]	Extinction amplitude
Ag_{α}	3.64	340.65	0.716	0.240±0.001
Ag^{0}	3.20	387.5	0.695	0.137±0.001
Ag_{n}	2.75	450.90	0.981	0.210±0.001

3.3 Demonstration of laser-creation of optical waveguides

After looking at local properties, as displayed in Figs. 3 and 4, we performed DLW along the length of the sample (7 mm), at constant depth and irradiation parameters (Fig. 5). As a proof-of-concept demonstration of waveguiding, only the waveguide produced at 300 µm/s is shown. A top-view fluorescence image of the waveguiding structure is shown in Fig. 5(a) (excitation at 405 nm), showing a double-track fluorescent structure that corresponds to the spatial distribution of laser-induced silver NC's. The corresponding top-view phase image is given in Fig. 5(b), showing also a double-track index structure spatially correlated to the position of the NC's double-track distribution. The produced index change structure is therefore sustained by the laser-induced NC's, locally showing a positive index change along the double-track structure of the order of magnitude of 10^{-3}, which is compatible with waveguiding behavior. The observed inhomogeneities along the fluorescence and index change distributions are due to mechanical vibrations during the DLW process, which can be fully removed to create perfectly smooth double-track distributions [**17**]. Fig. 5(c) depicts the lateral cross-section of the index change distribution, highlighting the double-track structure sustained by the silver cluster distribution, with a typical amplitude of 1.3×10^{-3} index change. Note that the full width at half maximum (FWHM) of each track is about 600 nm, which results from the convolution the phase imaging point spread function, as the refractive index does not match the ideal index of 1.518 for ideal imaging conditions with corrected spherical aberrations. Each individual track is thus much thinner than 600 nm. The onset of Fig. 5(c) shows that the waveguide depth was about 200 µm below the glass surface. The depicted near-field waveguided profile, imaged at the output facet of the glass sample, for a He-

Ne radiation at 633 nm, shows the overlapping of two ellipsoid-shaped tracks, similarly to the pioneer observation of Abou Khalil *et al.* in silver-containing phosphate glasses [17].

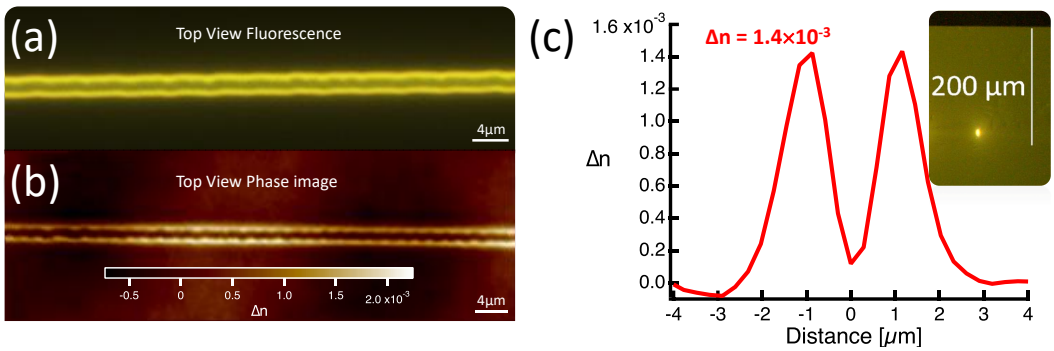

Figure 5. (a) Fluorescence image (top view) of a double-track fluorescent structure corresponding to laser-induced silver NC's (excitation at 405 nm); corresponding phase image (top view) of such double-track structure showing a correlative positive index change modification; (c) cross-section of the waveguiding structure, depicting the double-track profile and index changes up to 1.3×10^{-3}, and near-field waveguided profile (side view) at the output facet of the glass sample at 200 µm below surface.

3.4 Original management of the silver reservoir in the fluorophosphate glass

Bellec *et al.* have shown that in the case of silver-containing phosphate glasses the central part of the structuring laser beam tends to photo-dissociate silver NC's that had been created by a previous laser pass [34]. While the successive overlapping of laser passes destroys laser NC's, it does not allow for the significant novel production of fluorescent silver clusters. It demonstrates that the available silver reservoir for laser structuring and associated silver NC's production is mostly fully consumed during the first laser pass in such oxide glass (composition $40P_2O_5$-$55ZnO$-$1Ga_2O_3$-$4Ag_2O$ mol%). This effect is highlighted in Fig. 6(a) where fluorescent structures are shown with distinct interdistances between two successive laser passes. For interdistances of 5 µm and 1 µm, the beam diameter is typically smaller or similar to the inner separation between a double-track structure, so that the resulting pattern shows a bright fluorescence (excitation at 375 nm). However, the interdistances of 0.5 µm leads to a strong overlapping between the intense central laser beam and pre-created silver NC's,

which dominantly leads to the global erasure of produced silver NC's and finally to a poorly fluorescent pattern. While performing re-irradiation and erasing of pre-created silver NC's, the reservoir of available silver species for silver NC's is not refreshed nor refilled.

If now considering the fluorophosphate glass, the management of the silver reservoir and its re-use with successive laser passes shows a remarkably distinct behavior. Indeed, while interdistances of 5 µm and 1 µm lead to similar behavior than that of the oxide phosphate glass, the 0.5 µm interdistance still leads to a globally intense fluorescent pattern, as seen in Fig. 6(b), unlike the silver-containing phosphate glasses. Therefore, the management of the silver reservoir behaves differently, with two possible interpretations: (i) a much larger available silver species may exist in the case of the fluorophosphate glass so that the successive overlapping laser passes did not singificantly consume the whole available silver reservoir; or (ii) the successive laser overlapping irradiation may regenerate the silver reservoir, so that it is still possible to re-write, even after several laser passes. The presence of a co-mobile elements, namely Fluorine F^- ions but also Sodium Na^+ ions, should be emphasized in the fluorophosphate glass, which may significantly affect both the silver species mobility and their subsequent chemical reactivity, but also the management of the silver reservoir. Therefore, the management of the silver reservoir behaves differently, with two possible interpretations. On the one hand, a much larger available silver species may exist in the case of the fluorophosphate glass so that the successive overlapping laser passes did not singificantly consume the whole available silver reservoir. Indeed, the amount of available silver species corresponds here to the useful fraction of the total silver ion reservoir that can truly be sollicited and involved in the laser modification process. The initial silver ion concentrations were 14.9×10^{20} cm^{-3} and 8.5×10^{20} cm^{-3} for the oxide and fluorophoshate glasses, respectively. Thus, even though the total silver ion reservoir is larger in the oxide glass than that of the fluorophoshate glass, the useful silver ion reservoir available for material modification may possibly be larger in the fluorophoshate matrix. On the other hand, the successive laser overlapping irradiation may regenerate the silver reservoir, so that it is still possible to re-write, even after several laser passes. The presence of a co-mobile elements, namely Fluorine F^- ions but also Sodium Na^+ ions, should be emphasized in the fluorophosphate

glass, which may significantly affect both the silver species mobility and their subsequent chemical reactivity, but also the management of the silver reservoir. Besides, despite their high mobility, Na^+ ions can contribute to enhance the mobility of Ag^+ ions and its subsequent photo-chemical reactivity to growth fluorescent clusters, as recently reported in a fluorine-free silver-containing sodium gallophosphate glass series with fixed Ag^+ cationic concentration [**22**]. Moreover, beyond the question of Na^+ ion mobility, the introduction of such sodium ions may also affect the glass matrix itself, which can affect in turn influence the management of the silver reservoir [**5**,**22**]. Therefore, such presence of co-mobile species should require further attention, to optimally design the photo-sensitivity of silver-containing photonic glasses for fs laser structuring.

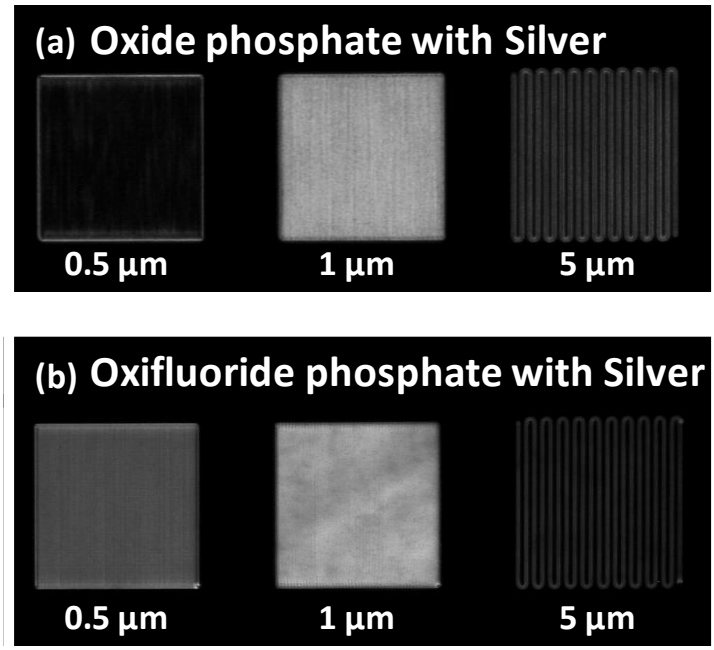

Figure 6. Fluorescence wide-field imaging (excitation at 375 nm) for distinct interdistances between each laser pass: (a) case of our standard oxide silver-containing phosphate glass; (b) case of our new silver-containing fluorophosphate glass under study, remarkably showing the pioneer non-vanishing fluorescent behavior for strong overlapping conditions with interdistances of 0.5 µm, contrarily to the oxide glass.

4. Conclusion

We have reported on the synthesis of a silver-containing fluorophosphate glass that shows photo-sensitivity under femtosecond laser irradiation. This has led to the efficient sub-microscale three-dimension production of highly fluorescent structures, with linear absorption coefficients reaching the 10 000 cm^{-1} order of magnitude. Furthermore, a positive index change distribution has been reported, leading to the demonstration of optical waveguiding. Finally, we have reported the pioneer observation of re-writing behavior of fluorescent silver clusters in our new silver-containing fluorophosphate glass, which was not accessible using standard oxide phosphate glasses. Indeed, the consideration of additional co-mobile species, namely fluorine and/or sodium ions, with silver species may pave the way to better tailored silver-containing glass compositions, so as to increase the available silver reservoir and to enhance the material photosensitivity under laser structuring. This property should lead to the design of innovative photonic devices such as photonic optical circuits, evanescent sensors or 3D high-density optical data storage.

Acknowledgments: This study was carried out with financial support from the frame of 'the Investments for the future' Programme IdEx Bordeaux – LAPHIA (ANR-10-IDEX-03-02), as well as in the frame of the ANR program, Funder Id: 10.13039/501100001665 (N°ANR-17-CE08-0042-01). This study was also supported by the French Region Nouvelle Aquitaine, with the program N° 2016 – 1R10107. Finally, the authors acknowledge the Brazilian agency FAPESP (grants numbers #2018/09296-3, #2016/16343-2 and #2013/07793-6) for financial support.

References

1. R. R. Gattass and E. Mazur, Nat. Photonics, 2, (2008), 219–225.
2. M. Malinauskas, A. Žukauskas, S. Hasegawa, Y. Hayasaki, V. Mizeikis, R. Buividas and S. Juodkazis, Light: Science & Applications, 5, (2016), e16133
3. S. Gross and M. J. Withford, Nanophotonics, 4(3), (2015), 332–352.
4. A. Royon, Y. Petit, G. Papon, M. Richardson and L. Canioni, Opt. Mater. Expr., 1, (2011), 866–882. [Invited]

5. Y. Petit, S. Danto, T. Guérineau, A. Abou Khalil, A. Le Camus, E. Fargin, G. Duchateau, J.-P. Bérubé, R. Vallée, Y. Messaddeq, T. Cardinal and L. Canioni, Adv. Opt. Techn., 7(5), (2018), 291-309.
6. J. Qiu, K. Miura, K. Hirao, J. Non-Cryst. Solids, 354, (2008), 1100–1111.
7. L. A. Siiman J. Lumeau L. B. Glebov, J. Non-Cryst. Solids, 354, (2008), 4070–4074.
8. M. Vangheluwe, Y. Petit, N. Marquestaut, A. Corcoran, E. Fargin, R. Vallée, T. Cardinal and L. Canioni, Opt. Mater. Expr., 6, (2016), 743–748.
9. W.-E. Lu, Y.-L.Zhang, M.-L. Zheng, Y.-P. Jia, J. Liu, X.-Z. Dong, Z.-S. Zhao, C.-B. Li, Y. Xia, T.-C. Ye, and X.-M. Duan, Opt. Mater. Expr., 3, (2013), 1660–1673.
10. I. Díez, M. Pusa, S. Kulmala, H. Jiang, A. Walther, A. S. Goldmann, A. H. E. Muller, O. Ikkala, and R. H. A. Ras, Angew. Chem., 48, (2009), 2122–2125.
11. A. Malakho, E. Fargin, A. Delestre, C. André, T. Cardinal, M. Lahaye, V. Rodriguez, M. Couzi, F. Adamietz, L. Canioni and A. Royon, J. Appl. Phys., 104, (2008), 053114.
12. G. Papon, Y. Petit, N. Marquestaut, A. Royon, M. Dussauze, V. Rodriguez, T. Cardinal and L. Canioni, Opt. Mater. Expr., 3, (2013), 1855–1861.
13. G. Papon, N. Marquestaut, Y. Petit, A. Royon, M. Dussauze, V. Rodriguez, T. Cardinal, and L. Canioni, J. Appl. Phys., 115, (2014), 113103-1.
14. C. Hua, X. Zhao, E. Yue, B. Pun, H. Lin, RSC Adv., 7, (2017), 55691-55701.
15. H. Fares, T. Castro, J. Resges Orives, D. Faza Franco and M. Nalin, RSC Adv., 7, (2017), 44356–44365.
16. J. W. Chan, T. R. Huser, S. H. Risbud, J. S. Hayden, and D. M. Krol, Appl. Phys. Lett., 82, (2003), 2371.
17. A. Abou Khalil, J.-P. Bérubé, S. Danto, J.-C. Desmoulin, T. Cardinal, Y. Petit, R. Vallée and L. Canioni, Scientific Reports, 7, (2017), 1–9.
18. G. Yu. Shakhgildyan, A.S. Lipatiev, M.P. Vetchinnikov, V.V. Popova, S.V. Lotarev, N.V. Golubev, E.S. Ignat'eva, M.M. Presniakov, V.N. Sigaev, J. Non-Cryst. Solids, 1, (2018), 634–642.
19. A. S. Kuznetsov, J. J. Velázquez, V. K. Tikhomirov and J. Mendez-Ramos. Appl. Phys. Lett., 101, (2012), 251106/1–5.
20. Y. Liu, B. Zhu, L. Wang, J. Qiu, Y. Dai, and H. Ma, Appl. Phys. Lett., 92 (2008), 121113.

21. S. Richter, C. Miese, S. Doring, F. Zimmermann, M. J. Withford, A. Tunnermann and S. Nolte, Opt. Mater. Expr., 3, (2013), 1161–1166.
22. T. Guérineau, L. Loi, Y. Petit, S. Danto, A. Fargues, L. Canioni, and T. Cardinal, Opt. Mater. Expr., 8, (2018), 3748-3760.
23. E. Smetanina, B. Chimier, Y. Petit, N. Varkentina, E. Fargin, L. Hirsch, T. Cardinal, L. Canioni, and G. Duchateau, Phys. Rev. A, 93, (2016), 013846.
24. A. Royon, K. Bourhis, M. Bellec, G. Papon, B. Bousquet, Y. Deshayes, T. Cardinal, and L. Canioni, Adv. Mater., 22, (2010), 5282–5286.
25. S. Danto, F. Désévédavy, Y. Petit, J.-C. Desmoulin, A. Abou Khalil, C. Strutynski, M. Dussauze, F. Smektala, T. Cardinal, and L. Canioni, Adv. Opt. Mater., 4, (2016), 162–168.
26. H. Fares, S. N. C. Santos, M. V. Santos, D. F. Franco, A. E. Souza, D. Manzani, C. R. Mendonça and M. Nalin, RSC Adv., 7, (2017), 55935–55944.
27. V. A. Aseev, P. A. Burdaev, E. V. Kolobkova and N. V. Nikonorov, Glass Phys. Chem., 38, (2012), 366–372.
28. T. Djouama, M. Poulain, B. Bureau, R. Lebullenger, J. Non-Cryst. Solids, 414, (2015), 16–20.
29. P. Kunwar, J. Hassinen, G. Bautista, R. H. A. Ras and J. Toivonen, ACS Nano, 2014, 8, 11165–1117.
30. W. Chen, A. G. Joly, and J. Roark, Phys. Rev. B, 65, (2002), 245404.
31. A.S. Kuznetsov, V.K. Tikhomirov, M.V. Shestakov, V.V. Moshchalkov, Nanoscale, 5, (2013), 10065-10075.
32. V. K. Tikhomirov, V. D. Rodríguez, A. Kuznetsov, D. Kirilenko, G. Van Tendeloo and V. V. Moshchalkov, Opt. Expr., 18, (2010), 22032–22040.
33. N. Marquestaut, Y. Petit, A. Royon, P. Mounaix, T. Cardinal, and L. Canioni, Adv. Funct. Mat. 24(37), (2014), 5824-5832.
34. M. Bellec, A. Royon, K. Bourhis, J. Choi, B. Bousquet, M. Treguer, T. Cardinal, J.-J. Videau, M. Richardson, and L. Canioni, J. Phys. Chem. C, 114, (2010), 15584–15588.